Biophysical Journal
Article

Biophysical Society

# Orthosteric and Allosteric Activation of Human 5-HT$_3$A Receptors

Noelia Rodriguez Araujo,[1] Camila Fabiani,[1] Albano Mazzarini Dimarco,[1] Cecilia Bouzat,[1,*] and Jeremías Corradi[1,*]

[1]Instituto de Investigaciones Bioquímicas de Bahía Blanca (INIBIBB), Departamento de Biología, Bioquímica y Farmacia, Universidad Nacional del Sur (UNS)-Consejo Nacional de Investigaciones Científicas y Técnicas (CONICET), Bahía Blanca, Argentina

ABSTRACT The serotonin type 3 receptor (5-HT$_3$) is a ligand-gated ion channel that converts the binding of the neurotransmitter serotonin (5-HT) into a transient cation current that mediates fast excitatory responses in peripheral and central nervous systems. Information regarding the activation and modulation of the human 5-HT$_3$ type A receptor has been based only on macroscopic current measurements because of its low ion conductance. By constructing a high-conductance human 5-HT$_3$A receptor, we here revealed mechanistic information regarding the orthosteric activation by 5-HT and by the partial agonist tryptamine, and the allosteric activation by the terpenoids, carvacrol, and thymol. Terpenoids potentiated macroscopic currents elicited by the orthosteric agonist and directly elicited currents with slow-rising phases and submaximal amplitudes. At the single-channel level, activation by orthosteric and allosteric agonists appeared as openings in quick succession (bursts) that showed no ligand concentration dependence. Bursts were grouped into long-duration clusters in the presence of 5-HT and even longer in the presence of terpenoids, whereas they remained isolated in the presence of tryptamine. Kinetic analysis revealed that allosteric and orthosteric activation mechanisms can be described by the same scheme that includes transitions of the agonist-bound receptor to closed intermediate states before opening (priming). Reduced priming explained the partial agonism of tryptamine; however, equilibrium constants for gating and priming were similar for 5-HT and terpenoid activation. Thus, our kinetic analysis revealed that terpenoids are efficacious agonists for 5-HT$_3$A receptors. These findings not only extend our knowledge about the human 5-HT$_3$A molecular function but also provide novel insights into the mechanisms of action of allosteric ligands, which are of increasing interest as therapeutic drugs in all the superfamily.

SIGNIFICANCE The serotonin type 3 receptor (5-HT$_3$) is a ligand-gated ion channel that converts the binding of serotonin into a cationic current, thus mediating fast excitatory responses in peripheral and central nervous systems. Natural compounds, such as terpenoids, modulate receptor activity by binding to different (allosteric) sites. The mechanism of allosteric activation remains unknown, despite the therapeutic importance of allosteric ligands. By combining expression of human 5-HT$_3$A receptors with single-channel recordings and kinetic modeling we revealed new mechanistic information regarding allosteric activation by two terpenoid natural compounds, carvacrol and thymol, and determined how this mechanism relates to that elicited by serotonin. The understanding of how drugs and natural compounds acting from different sites modify receptor molecular function contributes to drug design.

## INTRODUCTION

Serotonin type 3 receptor (5-HT$_3$) is a ligand-gated ion channel that belongs to the Cys-loop receptor family along with nicotinic, glycine, and GABA receptors. They are homopentameric or heteropentameric receptors that contain an extracellular domain, which carries the agonist binding sites at subunit interfaces; a transmembrane domain, which comprises the pore and it is formed by four $\alpha$-helices of each subunit (TM1–TM4), with TM2 segments forming the walls of the ion channel; and an intracellular domain, which is formed by the intracellular loop between TM3 and TM4 of each subunit and is implicated in trafficking, modulation, and ion conductance (1–3).

Human 5-HT$_3$ receptors are located in the peripheral and enteric nervous systems, in which they play a role

*Submitted April 15, 2020, and accepted for publication August 24, 2020.*

*Correspondence: inbouzat@criba.edu.ar or jcorradi@cribar.edu.ar

Noelia Rodriguez Araujo and Camila Fabiani contributed equally to this work.

Editor: Andrew Plested.

https://doi.org/10.1016/j.bpj.2020.08.029

in peristalsis, gut motility, and in several sympathetic, parasympathetic, and sensory functions. They are also found in many areas of the central nervous system, with roles in a variety of functions including emesis, cognition, and anxiety (4).

Five human 5-HT$_3$ subunits (*5HT3A–E*) have been identified to date (5–7). The *5HT3A* subunit is the only one that can form homomeric receptors (5-HT$_3$A) (8,9), whereas *5HT3B–E* subunits form heteromeric receptors by assembling with the *5HT3A* subunit (5,6,10–12). The subunit composition and stoichiometry of native receptors remain mostly unknown.

Native homomeric 5-HT$_3$A receptors have a very low ion channel conductance that has prevented the detection of single-channel openings (1,8). The combined mutations of three residues in the intracellular domain increase the ion channel conductance, allowing single-channel events to be detected under the cell-attached patch-clamp configuration (1,13,14). Thus, this high-conductance receptor model (5-HT$_3$A$_{HC}$) is a valuable tool to study in detail mechanisms of receptor activation and modulation. Taking advantage of the high-conductance receptor, we have previously generated models that describe the kinetics of activation by full and partial orthosteric agonists (14,15), and of inhibition by negative allosteric modulators of the mouse 5-HT$_3$A receptor (16). The kinetic analysis of the mouse 5-HT$_3$A receptor showed that two or three agonist binding sites have to be occupied for maximal response and proposed the existence of intermediate preactivated closed states (14,17). Intermediate preactivated closed states have been first described in glycine and nicotinic receptors. It has been proposed that the efficacy of an agonist is mainly determined by its ability to change the receptor conformation from a closed state to these preactivated states (14,15,18–20).

In human health, 5-HT$_3$ competitive antagonists, like granisetron, alosetron, ondansetron, and palanosetron, are used to alleviate gastrointestinal symptoms associated with chemotherapy, anesthesia, and irritable bowel syndrome (4,21). They are also considered as promising therapy for the treatment of other disorders like schizophrenia, depression, anxiety, addictions, cognitive disfunction, and eating disorders (4,22).

In addition to the orthosteric ligands, several compounds have been reported to allosterically modulate 5-HT$_3$A function. They can act as negative allosteric modulators of 5-HT$_3$ receptors, such as alkaloids (23), steroids (24), cannabinoids (25), and terpenes (26,27); as positive allosteric modulators (PAMs), like alcohol (28), 5-hydroxyindole (29), and 5-chloroindole (30); and as ago-PAMs, which are capable of activating in the absence of an orthosteric agonist and potentiating in its presence, like the terpenoids carvacrol and thymol (31,32).

Terpenoids act as allosteric modulators of 5-HT$_3$A receptors by binding probably to a transmembrane site. Whereas some of them act as negative modulators, like menthol, citronellol, and boldine (26,27,32,33), others, like carvacrol and thymol, act as ago-PAMs (31,32). This information shows how drugs with high structural similarities can exert divergent effects on the same receptor, reinforcing the idea that subtle structural modifications can result in multiple different pharmacological effects.

Allosteric ligands have attracted high attention as promising therapeutic and research tools because they show higher specificity and cover a wider range of effects compared to orthosteric ligands, and, in the case of allosteric modulators lacking agonist activities, their effects follow the temporal activity exerted by the natural endogenous neurotransmitter (34). Thus, the elucidation of sites and mechanisms of action of allosteric compounds is of intense research interest.

During the last years, important efforts have been made toward the elucidation of the structural and mechanistic bases of activation of Cys-loop receptors, which have provided insights into the processes involved in neurotransmitter activation via the orthosteric sites (19,35–37). In contrast, the molecular mechanism underlying the allosteric activation remains an enigma.

Information of the molecular function of human 5-HT$_3$A receptor has lagged behind because of its low conductance. To overcome this gap, we here constructed the high-conductance form of the human 5-HT$_3$A receptor and explored by macroscopic current and single-channel recordings the activation kinetics by orthosteric agonists, full (5-HT) and partial (tryptamine), as well as the kinetics of activation and modulation by the allosteric ligands carvacrol and thymol.

Our results show the first microscopic description of the allosteric activation and modulation of the human 5-HT$_3$A receptor and remark the differences and similarities with the activation through the neurotransmitter binding sites. This study enhances the importance of single-channel recordings for a deep understanding of drug action in ligand-gated ion channels. Overall, we here provide novel, to our knowledge, insights into the molecular function of human 5-HT$_3$A and, in particular, into the mechanisms of activation and modulation by allosteric ligands, which are of interest as potential therapeutic drugs in all the superfamily.

## MATERIALS AND METHODS

### Materials

All compounds were obtained from Sigma-Aldrich (St Louis, MO). Carvacrol (5-isopropyl-2-methylphenol) and thymol (2-isopropyl-5-methylphenol) were prepared as stock solutions in DMSO (300 mM) and stored at −20°C, followed by dilution in buffer at the concentration required for the experiment. Final DMSO concentration was <1% in all cases. Serotonin (3-(2-aminoethyl)-5-hydroxyindole hydrochloride) and tryptamine (3-(2-aminoethyl)indole hydrochloride) solutions were prepared in buffer.

### Expression of high-conductance 5-HT$_3$A receptors

The high-conductance form of the human serotonin type 3A receptor (5-HT$_3$A$_{HC}$) was obtained by mutating three arginine residues (R432, R436, and R440) responsible for the low conductance to glutamine, aspartic

acid, and alanine as described before for the mouse 5-$HT_3$A receptor (14,38). Point mutations were carried out using the Quik Change Kit (Stratagene, La Jolla, CA) and were confirmed by sequencing. BOSC23 cells, derived from HEK 293 cells, were transfected with the high-conductance form of *5HT3A* subunit cDNA (*5HT3A*$_{HC}$) and a plasmid-encoding green fluorescent protein to allow identification of transfected cells (14,38).

## Patch-clamp recordings

Single-channel currents were recorded in the cell-attached configuration at 20°C. The bath and pipette solutions contained 142 mM KCl, 5.4 mM NaCl, 0.2 mM $CaCl_2$, and 10 mM HEPES (pH 7.4). Agonists were added to the pipette solution. Single-channel currents were recorded using an Axopatch 200B patch-clamp amplifier (Molecular Devices, San Jose, CA), digitized at 200 kHz and low-pass filtered at a cutoff frequency of 10 kHz using a computer interface Instrutech ITC-18 (HEKA Instruments, Holliston, MA). Single-channel events were idealized by the half amplitude threshold criterion using the program QuB 2.0.0.28 (QuB suite, www.qub.buffalo.edu; State University of New York, Buffalo, NY) with digital low-pass filter at 9 kHz. The open and closed durations were estimated from the idealized recordings by the maximal interval likelihood (MIL) function in QuB with a dead time of 0.03 ms, which is the interval duration below which events cannot be resolved (39,40). Therefore, only events longer than the dead time were used to construct the duration histograms. This analysis was performed on the basis of a kinetic model whose probability density function curves properly described the corresponding histograms after the maximal likelihood criteria. Bursts and clusters of channel openings were identified as a series of closely separated openings (more than five) preceded and followed by closings longer than a critical duration. Clusters corresponded to the longest-duration stretches of successive openings originated from the same receptor molecule. They were composed by shorter episodes of successive openings called bursts. The critical duration was obtained by the point at which the exponential component that described the longer closings within bursts (or clusters) intersected the following component, thus minimizing the fraction of misclassified closed events (41). For defining clusters, the critical duration was taken as the point of intersection between the third and fourth closed component and its value was ~10–20 ms. For bursts, the critical closed duration was defined between the second and third component and was ~0.5–1.0 ms. A 10–20 time increase in the critical time for defining clusters did not affect the mean cluster duration, indicating that clusters were well defined. For tryptamine, only isolated bursts were clearly defined. A 10–20 time increase in the critical time for burst resolution did not affect the mean burst duration, indicating that bursts were separated by longer closed periods and that clusters could not be distinguished.

The corresponding critical closed duration was used as a terminator in QuB to chop the recording and create a list of bursts or clusters. Cluster duration, burst duration, and open probability within clusters and within bursts were plotted and clustered using the K-Means algorithm to define the corresponding mean values.

Macroscopic currents were recorded in the whole-cell configuration. The pipette solution contained 134 mM KCl, 5 mM EGTA, 1 mM $MgCl_2$, and 10 mM HEPES (pH 7.3). The extracellular solution (ECS) contained 150 mM NaCl, 0.5 mM $CaCl_2$, 10 mM HEPES (pH 7.4). For generating serotonin and tryptamine dose-response curves, 1.4-s pulses of ECS containing different concentrations of each agonist were applied. For carvacrol and thymol, the agonist pulse was extended up to 8 s because of their slower rising phase. The solution exchange time was estimated by the open pipette method as described before (42). This method consists in applying a pulse of 50% diluted ECS to an open patch pipette, which produces a sudden change in the current measured by the patch-clamp amplifier. After proper adjustment of the electrode position, the current jump in our system varied between 0.1 and 1 ms.

Macroscopic currents were acquired by WinWCP V5.3.7 (Strathclyde Institute of Pharmacy & Biomedical Sciences, Glasgow, UK), filtered at 5 kHz, digitized at 20 kHz, and analyzed using Clampfit 10.4 (Molecular Devices, San Jose, CA). Each current represents the average from three to five individual traces obtained from the same seal. The rise time corresponds to the time taken by the current to increase from 10 to 90% of its maximal value ($t_{10–90\%}$). For 5-HT-activated currents, decays were fitted by a double exponential function according to the equation:

$$I_{(t)} = I_{fast}\left[\exp\left(-t / \tau_{fast}\right)\right] + I_{slow}\left[\exp\left(-t / \tau_{slow}\right)\right] + I_{\infty}$$

in which $I_0$ and $I_\infty$ are peak and the steady-state current values, respectively, and $\tau$ are the decay time constants.

$EC_{50}$ values were obtained by fitting dose-response curves with the Hill equation.

## Single-channel kinetic analysis

For kinetic modeling, clusters or bursts were selected on the basis of their distribution of mean duration and open probability (14,15). The resulting open and closed intervals, from single patches at different ligand concentrations, were analyzed according to a kinetic scheme using the MIL algorithm from the QuB Software (39,40) (QuB suite, www.qub.buffalo.edu; State University of New York, Buffalo, NY) as described before (14,15). The model and the estimated rates were accepted if the resulting probability density functions correctly described the experimental open- and closed-duration histograms.

## Statistical analysis

Data were presented as mean ± SD. Statistical comparisons were performed with the Student's *t*-test. Statistically significant differences were established at *p*-values $<0.05$.

# RESULTS

## Activation of the human 5-$HT_3A_{HC}$ receptor by orthosteric and allosteric ligands at the macroscopic level

The human 5-$HT_3$A receptor channel has a very low ion conductance that impairs the detection of single-channel openings from cell-attached patches (1). To overcome this limitation, we mutated three residues at the intracellular domain to yield the high-conductance form of the human 5-$HT_3$A receptor (5-$HT_3A_{HC}$), as previously described for the mouse 5-$HT_3$A receptor (14–16). To characterize the macroscopic activation properties, whole-cell currents were recorded from BOSC23 cells transfected with the human *5HT3A*$_{HC}$ subunit cDNA. Rapid application to the cells of a saturating 5-HT concentration (100 $\mu$M) elicited macroscopic currents that decayed during the pulse of agonist application (Fig. 1, *A* and *C*). The rise time measured from the $t_{10–90\%}$, was 10 ± 4 ms and decays were fitted by two exponential components, with time constants of 92 ± 20 and 1100 ± 900 ms ($n = 5$). These values were similar to those of wild-type 5-$HT_3$A receptor currents elicited by 100 $\mu$M 5-HT ($t_{10–90\%}$ of 16 ± 6 ms and decay time constants of 120 ± 50 and 700 ± 400 ms ($n = 5$)). The concentration-response curve for the high-conductance 5-$HT_3$A resulted in an $EC_{50}$-value of 2.6 ± 0.1 $\mu$M

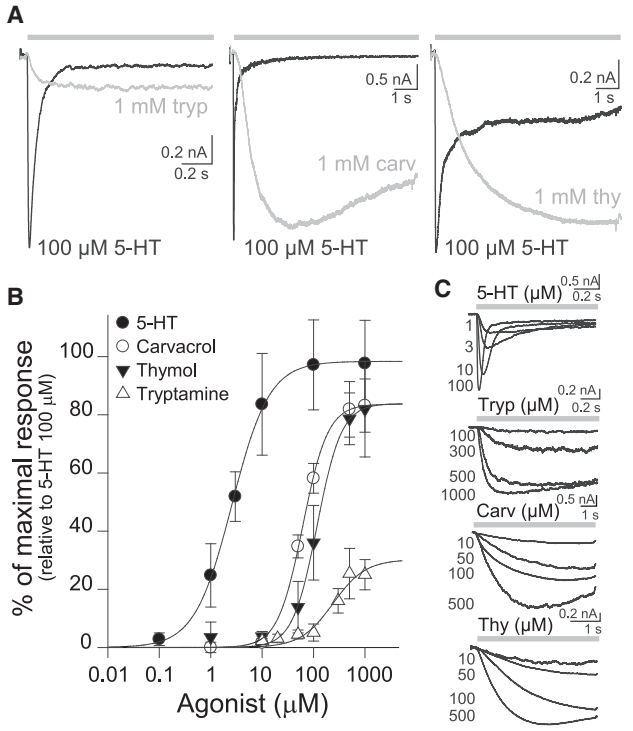


FIGURE 1 Macroscopic currents from human 5-HT$_3$A$_{HC}$ receptors elicited by orthosteric and allosteric agonists. (*A*) Typical macroscopic currents elicited by 5-HT (*black currents*), and compared to those elicited by tryptamine, carvacrol, or thymol (*gray currents*) in the same cell at the indicated concentrations. The holding potential is −50 mV. (*B*) Dose-response curves for the 5-HT$_3$A$_{HC}$ receptor. Current amplitudes were normalized to those of 100 $\mu$M 5-HT-elicited currents. Data points are the mean values ± SD from three cells for each condition. (*C*) Typical whole-cell currents obtained at the different agonist concentrations.

($R^2 = 0.99$, Fig. 1 *B*), similar to that previously reported for the wild-type human 5-HT$_3$A receptor ($EC_{50}$ = 1–2 $\mu$M) (12,31).

We also explored macroscopic activation of human 5-HT$_3$A$_{HC}$ receptor by tryptamine, which is a partial agonist of mouse and human 5-HT$_3$A receptor (15,43). Compared to 5-HT, tryptamine-elicited currents showed a slower activation phase (Fig. 1, *A* and *C*) and did not decay during the time of agonist application (1.4 s). The rise time obtained at a saturating concentration of tryptamine (1 mM), measured from the $t_{10–90\%}$, was 200 ± 100 ms (Fig. 1 *A*). The dose-response curve showed an $EC_{50}$ of 197 ± 50 $\mu$M and a maximal response of 27 ± 3% compared to that elicited by 100 $\mu$M 5-HT ($R^2 = 0.98$), indicating that tryptamine is a very weak agonist for the human 5-HT$_3$A$_{HC}$ receptor (Fig. 1 *B*). These values were in line with those reported for the wild-type human 5-HT$_3$A receptor ($EC_{50}$ of 100–200 $\mu$M and ∼27% of maximal response (43)). Thus, our macroscopic characterization indicates that the high-conductance receptor behaves similarly to the wild-type 5-HT$_3$A receptor.

Carvacrol and thymol are two phenolic monoterpenes that have been macroscopically characterized as allosteric partial agonists and positive allosteric modulators of the human 5-HT$_3$A receptor (ago-PAMs) (31,32). We recorded macroscopic currents elicited by these ligands at a concentration range from 1 $\mu$M to 1 mM (Fig. 1, *B* and *C*). Terpenoid concentrations higher than 1 mM produced membrane instability and could not be evaluated. The profiles of macroscopic responses were similar for both agonists but different to those elicited by 5-HT. At all carvacrol and thymol concentrations, including at saturating concentrations, currents decayed slower than in the presence of 5-HT (Fig. 1 *A*), and full desensitization was not achieved during the time of agonist application (12 s) (Fig. 1 *C*). Currents elicited by saturating concentrations of carvacrol or thymol showed significantly slower activation phases with respect to that observed with 5-HT, with rise times ($t_{10–90\%}$) of 2280 ± 810 ms for 1 mM carvacrol ($n = 4$) and 4850 ± 750 ms for 1 mM thymol ($n = 5$) (Fig. 1 *A*). Concentration-response curves obtained for carvacrol and thymol showed higher $EC_{50}$-values (62 ± 2 and 117 ± 30 $\mu$M, respectively; $R^2 = 0.98$) and smaller maximal responses (84 ± 1 and 84 ± 8%, respectively) than those obtained by 5-HT (Fig. 1 *B*). These results were in close agreement with reports for the human wild-type 5-HT$_3$A receptor, showing $EC_{50}$ and maximal responses of ∼20 $\mu$M and ∼70%, and ∼50 $\mu$M and ∼80% for carvacrol and thymol, respectively (31).

These results revealed that the allosteric and orthosteric macroscopic activation of 5-HT$_3$A$_{HC}$ is indistinguishable from that of the wild-type receptor and that the high-conductance receptor is, therefore, a good model for studying activation at the single-channel level.

## Potentiation of the human 5-HT$_3$A$_{HC}$ receptor by carvacrol and thymol at the macroscopic level

To investigate the action of carvacrol and thymol as positive allosteric modulators of the human 5-HT$_3$A$_{HC}$, we recorded whole-cell currents activated by 50 $\mu$M tryptamine, a concentration close to the $EC_{20}$-value, with and without 10 $\mu$M carvacrol or 20 $\mu$M thymol, which correspond to concentrations close to their $EC_{10}$-values (Figs. 1 and 2). When 50 $\mu$M tryptamine was applied alone, typical responses showing slow activation and slow decay phases were detected, whereas application of thymol or carvacrol at these low concentrations elicited very small or negligible currents (Fig. 2 *A*). However, application of 50 $\mu$M tryptamine together with carvacrol (10 $\mu$M) or thymol (20 $\mu$M) produced marked potentiation of the macroscopic currents. For both compounds, peak currents increased ∼3-fold with respect to those elicited by tryptamine alone from the same cell (Fig. 2 *B*).

These results confirm that, in addition to their function as agonists, carvacrol and thymol act as positive allosteric modulators for the high-conductance form of human 5-HT$_3$A receptor and that the potentiating effect is evidenced at lower concentrations than the agonistic effect.

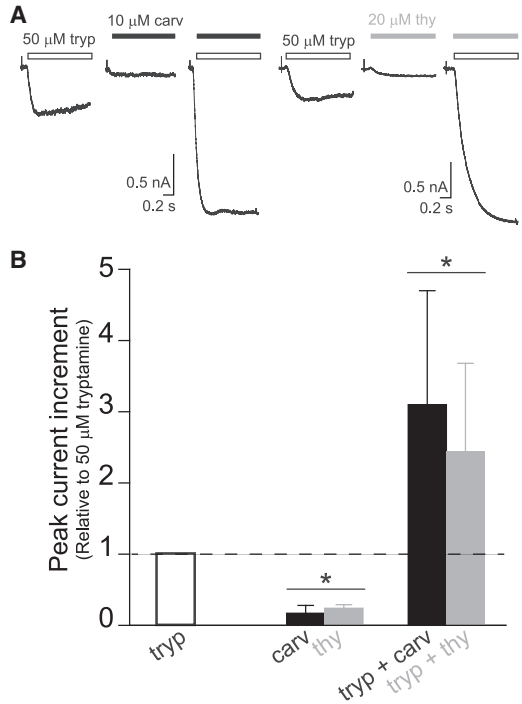


FIGURE 2 Potentiation of tryptamine-elicited currents by carvacrol and thymol. (*A*) Typical whole-cell currents elicited by rapid application of 50 $\mu$M tryptamine (*white*), 10 $\mu$M carvacrol (*black*), 20 $\mu$M thymol (*gray*), tryptamine + carvacrol, and tryptamine + thymol. The holding potential is −50 mV. (*B*) Increase of the peak of tryptamine-elicited currents by carvacrol (10 $\mu$M) or thymol (20 $\mu$M). Currents were elicited under the conditions shown in (*A*). Peak currents were normalized to those obtained with tryptamine in the same cell. The values correspond to the mean ± SD of 24 recordings for tryptamine, 4 for carvacrol, 3 for thymol, 12 for tryptamine + carvacrol, and 5 for tryptamine + thymol. *$p < 0.001$ with respect to tryptamine.

## Single-channel activation of human 5-HT$_3$A$_{HC}$ receptor by orthosteric agonists

Taking advantage of the high-conductance form of the human 5-HT$_3$A receptor, we explored the activation profile at the single-channel level.

At all 5-HT concentrations (1–30 $\mu$M), activation appeared as opening events of 4.5 ± 0.4 pA (−70 mV of membrane potential) in quick succession, forming bursts of high-open probability that, in turn, appeared grouped in well-defined long activation episodes named as clusters (Fig. 3; Fig. S1). Each cluster corresponds to the activation episode of a single receptor molecule that recovers from long-lived desensitization (See Materials and Methods for burst and cluster definitions). At 1 $\mu$M 5-HT, single-channel activity was observed as clusters of ~290 ms with high-open probability ($P_{open}$ ~0.94) (Fig. 3; Table 1). Clusters were composed by shorter stretches, called bursts, with mean durations of ~130 ms, which were defined as opening events in quick succession separated by closings briefer than 1 ms (See Materials and Methods, Fig. 3; Table 1). Open-time histograms were described by three distinct components whose durations were ~0.05, 0.40, and 23 ms (Fig. 3; Table 1).

At high 5-HT concentrations, a reduction in the duration of the slowest open component was observed (Table 1), probably because of the open-channel blockade (14). To describe this effect, we used the linear open-channel blockade scheme (44) and plotted the inverse of the open durations against agonist concentrations to obtain the corresponding forward blocking constant ($k_{+b}$) (Fig. S2). The obtained $k_{+b}$-value was $5.5 \times 10^6$ $M^{-1}$ $s^{-1}$ ($R^2$ = 0.98), similar to that observed for the mouse 5-HT$_3$A$_{HC}$ receptor (14).

Closed-time distributions were described by five to six components, the three briefest corresponding to closings within clusters (Fig. 3; Table 1). The mean duration values of the intracluster closings were constant from 1 to 30 $\mu$M 5-HT concentration range (Fig. S3; Table 1), indicating no agonist concentration dependence in the single-channel activation profile as reported before for the mouse 5-HT$_3$A$_{HC}$ receptor (14,15).

Compared to 5-HT, activation by tryptamine (10–100 $\mu$M) appeared mainly as short bursts that did not coalesce into long-duration clusters (Fig. 3). Visual inspection of the long recordings showed very few clusters. From 10 to 100 $\mu$M tryptamine, single-channel events appeared mainly as openings in quick succession grouped in high-$P_{open}$ bursts of ~30–60 ms (Table 1). The open-time histograms were described by only two components, the duration of the slowest open component being of ~6 ms at concentrations below 20 $\mu$M tryptamine (Table 1). Bursts were defined by a critical closed time of 0.8 ms, resulting in the mean durations described in Table 1, and they showed no significant agonist concentration dependence. To discard that bursts did not coalesce into longer clusters as in 5-HT activation, we also chopped the recordings with a 10- to 20-fold increased critical time (8–18 ms), similar to that used for calculating the mean cluster duration of 5-HT activated channels. Comparison of the mean cluster durations thus determined for all tryptamine concentrations (40 ± 28, 85 ± 23, 42 ± 14, and 42 ± 11 ms for 10, 20, 50, and 100 $\mu$M tryptamine, respectively) showed no statistically significant differences with the mean burst durations shown in Table 1 ($p > 0.05$ for all tryptamine concentrations), thus confirming that bursts appeared mostly isolated and discarding the presence of long clusters.

As for 5-HT, a reduction in the duration of the longest open component was observed with the increase in tryptamine concentration, which could be because of the open-channel blockade. The $k_{+b}$-value obtained as described above was $4.9 \times 10^6$ $M^{-1}$ $s^{-1}$ ($R^2$ = 0.98), similar to that observed for 5-HT (Fig. S2). Closed-time histograms were described by four to five components

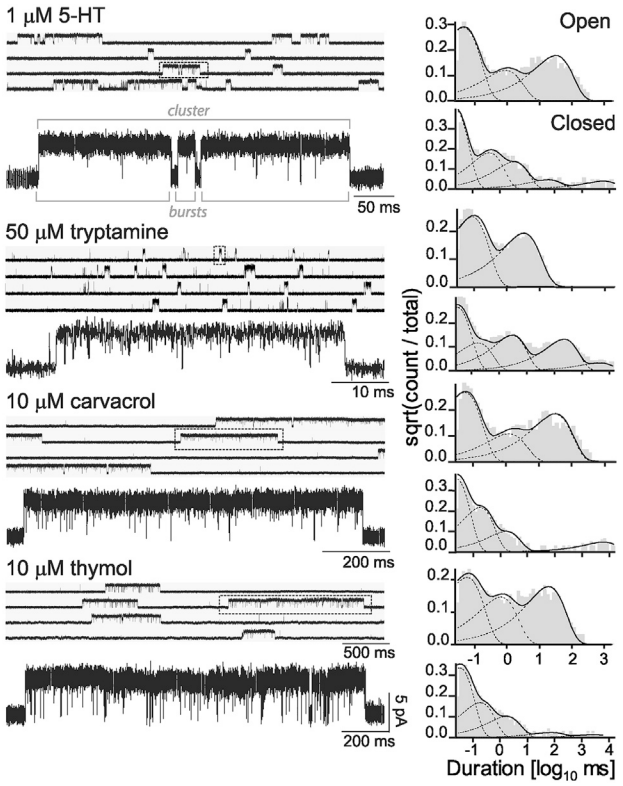


FIGURE 3 Single-channel currents evoked by 5-HT, tryptamine, carvacrol,or thymol. Shown is the typical single-channel traces obtained in the cell-attached configuration at −70 mV membrane potential. The filter is 9 kHz. Channel openings are shown as upward deflections. The stretch of openings that form a cluster, and the bursts within the cluster are indicated for 5-HT. In all channel traces, one cluster (for 5-HT, carvacrol and thymol) and one burst (for tryptamine) are marked in a box and shown below at a higher time resolution. At the right, representative open- and closed-duration histograms obtained from the analysis of the whole recording are shown for each condition.

(Fig. 3), and the mean durations of the two briefest closed components are shown in Table 1. Thus, the main differences of the single-channel pattern in the presence of tryptamine with respect to that in the presence of 5-HT are reduced open durations and lack of long-duration clusters.

## Single-channel activation by allosteric ligands

In the presence of different concentrations of carvacrol (5–50 $\mu$M) or thymol (5–100 $\mu$M) and in the absence of 5-HT, single-channel activity appeared as opening events with amplitudes similar to those of 5-HT elicited openings, which were grouped into long clusters as in the 5-HT activation pattern (Fig. 3).

Open-time histograms were fitted by three components that showed no agonist concentration dependence (Fig. 3; Table 1). At 5 $\mu$M, the mean durations of the open components were ∼0.02, ∼0.9, and ∼25 ms for carvacrol, and ∼0.07, ∼1.6, and ∼34 ms for thymol, which are in the same order as those of 5-HT activation (Table 1). Closed-time histograms were described by five to six components in which the three briefest components correspond to closings within clusters (Fig. 3; Table 1). Cluster durations and $P_{open}$ within clusters were constant at all tested concentrations. Interestingly, clusters elicited by the allosteric agonists were ∼6- to 10-fold longer than those observed with 5-HT (∼2500 and ∼1500 ms at 5 $\mu$M carvacrol and thymol, respectively) (Fig. 3; Table 1).

Thus, although the macroscopic profiles show that thymol and carvacrol behave as partial agonists of the human 5-HT$_3$A receptor, the single-channel pattern of the allosteric activation is more similar to that of 5-HT than to that of a genuine orthosteric partial agonist as tryptamine. In the presence of the allosteric agonists, 5-HT$_3$A$_{HC}$ receptors activate in high-$P_{open}$ long-duration clusters, which were markedly different to those elicited by tryptamine. Moreover, the mean durations of the activation episodes were significantly more prolonged for the allosteric ligands than for 5-HT.

## Single-channel potentiation of the human 5-HT$_3$A$_{HC}$ receptor by carvacrol and thymol

To evaluate potentiation by carvacrol and thymol, we recorded single-channel events elicited by tryptamine in the presence or absence of the terpenoids (Fig. 4). We used tryptamine as the agonist because we hypothesized that an increase in duration due to potentiation would be more clearly detected in tryptamine-elicited bursts than in 5-HT-elicited clusters, thus allowing a better distinction between activation and modulation processes.

We activated receptors by 50 $\mu$M of tryptamine in the presence of 10 $\mu$M of carvacrol or 10 $\mu$M of thymol. The recordings showed that channel activity appeared as long clusters of high $P_{open}$, whose values were similar to those in the presence of each allosteric agonist alone (Fig. 4; Table 1). However, for both conditions (tryptamine + carvacrol and tryptamine + thymol), open-time histograms were described by the same number of components and similar mean durations to those obtained in the presence of tryptamine alone (Fig. 4; Table 1). The appearance of longer clusters in the presence of terpenoids may be due to reduced desensitization due to their PAM action, a mechanism of action that has been described for PAMs of other Cys-loop receptors (34).

The reason why this mixed pattern occurs, showing brief openings as those elicited by tryptamine and long clusters as those elicited by carvacrol or thymol, remains unclear. One interesting and plausible explanation is that the open duration is mainly governed by the orthosteric agonist (tryptamine), whereas the cluster duration is mainly governed by the allosteric modulator (carvacrol or thymol). Alternatively, tryptamine may mainly act as an open-channel blocker when combined with terpenoids, thus inducing

**TABLE 1 Single-Channel Parameters of Human 5-HT$_3$A$_{HC}$ Receptors**

| Ligand | [$\mu$M] | $\tau_{OL}$ (ms) (Rel. Area) | $\tau_{OI}$ (ms) (Rel. Area) | $\tau_{OB}$ (ms) (Rel. Area) | $\tau_{CB}$ (ms) (Rel. Area) | $\tau_{CI}$ (ms) (Rel. Area) | $\tau_{CL}$ (ms) (Rel. Area) | Burst (ms) ($P_{open}$) | Cluster (ms) ($P_{open}$) | *n* |
|---|---|---|---|---|---|---|---|---|---|---|
| 5-HT | | | | | | | | | | |
| | 1 | 23 ± 6 | 0.40 ± 0.14 | 0.05 ± 0.01 | 0.02 ± 0.01 | 0.18 ± 0.10 | 2.6 ± 1.0 | 136 ± 54 | 287 ± 123 | 13 |
| | | (0.49 ± 0.19) | (0.20 ± 0.06) | (0.40 ± 0.20) | (0.46 ± 0.19) | (0.24 ± 0.12) | (0.30 ± 0.16) | (0.99 ± 0.01) | (0.94 ± 0.05) | |
| | 5 | 13 ± 4 | 0.20 ± 0.05 | 0.05 ± 0.01 | 0.03 ± 0.01 | 0.17 ± 0.04 | 1.7 ± 0.3 | 90 ± 34 | 221 ± 83 | 5 |
| | | (0.57 ± 0.08) | (0.14 ± 0.11) | (0.28 ± 0.06) | (0.42 ± 0.06) | (0.24 ± 0.07) | (0.22 ± 0.04) | (0.99 ± 0.01) | (0.91 ± 0.04) | |
| | 10 | 8.8 ± 2.4 | 0.17 ± 0.06 | 0.05 ± 0.01 | 0.03 ± 0.01 | 0.22 ± 0.13 | 2.2 ± 0.9 | 94 ± 53 | 246 ± 131 | 4 |
| | | (0.58 ± 0.09) | (0.11 ± 0.07) | (0.32 ± 0.10) | (0.43 ± 0.15) | (0.27 ± 0.11) | (0.21 ± 0.05) | (0.98 ± 0.01) | (0.89 ± 0.04) | |
| | 30 | 4.8 ± 0.6 | 0.24 ± 0.19 | 0.05 ± 0.02 | 0.03 ± 0.01 | 0.26 ± 0.16 | 2.2 ± 1.5 | 38 ± 10 | 98 ± 50 | 10 |
| | | (0.51 ± 0.10) | (0.17 ± 0.14) | (0.39 ± 0.10) | (0.37 ± 0.12) | (0.32 ± 0.08) | (0.27 ± 0.13) | (0.97 ± 0.01) | (0.78 ± 0.07) | |
| Tryptamine | | | | | | | | | | |
| | 10 | 6.9 ± 1.0 | 0.06 ± 0.03 | — | 0.03 ± 0.01 | 0.09 ± 0.01 | — | 29 ± 17 | — | 3 |
| | | (0.67 ± 0.28) | (0.33 ± 0.28) | — | (0.41 ± 0.26) | (0.12 ± 0.03) | — | (0.99 ± 0.01) | — | |
| | 20 | 5.5 ± 2.1 | 0.05 ± 0.02 | — | 0.03 ± 0.01 | 0.11 ± 0.06 | — | 62 ± 33 | — | 4 |
| | | (0.80 ± 0.23) | (0.09 ± 0.04) | — | (0.69 ± 0.22) | (0.10 ± 0.08) | — | (0.99 ± 0.01) | — | |
| | 50 | 3.2 ± 1.2 | 0.08 ± 0.03 | — | 0.03 ± 0.01 | 0.23 ± 0.10 | — | 26 ± 10 | — | 10 |
| | | (0.75 ± 0.12) | (0.21 ± 0.07) | — | (0.70 ± 0.13) | (0.21 ± 0.09) | — | (0.99 ± 0.01) | — | |
| | 100 | 1.7 ± 0.1 | 0.07 ± 0.01 | — | 0.04 ± 0.01 | 0.26 ± 0.07 | — | 30 ± 9 | — | 5 |
| | | (0.82 ± 0.17) | (0.18 ± 0.17) | — | (0.73 ± 0.16) | (0.05 ± 0.01) | — | (0.98 ± 0.01) | — | |
| Carvacrol | | | | | | | | | | |
| | 5 | 25 ± 5 | 0.90 ± 0.50 | 0.02 ± 0.01 | 0.02 ± 0.01 | 0.16 ± 0.08 | 1.2 ± 0.4 | 437 ± 133 | 2542 ± 998 | 3 |
| | | (0.59 ± 0.27) | (0.29 ± 0.30) | (0.10 ± 0.09) | (0.69 ± 0.16) | (0.21 ± 0.10) | (0.09 ± 0.07) | (0.99 ± 0.01) | (0.94 ± 0.02) | |
| | 10 | 38 ± 11 | 2.2 ± 1.8 | 0.09 ± 0.05 | 0.02 ± 0.01 | 0.12 ± 0.09 | 1.4 ± 0.9 | 472 ± 163 | 1734 ± 910 | 8 |
| | | (0.47 ± 0.20) | (0.26 ± 0.13) | (0.27 ± 0.17) | (0.54 ± 0.11) | (0.34 ± 0.10) | (0.09 ± 0.05) | (0.99 ± 0.01) | (0.98 ± 0.02) | |
| | 20 | 31 ± 17 | 1.2 ± 1.1 | 0.05 ± 0.02 | 0.02 ± 0.01 | 0.19 ± 0.12 | 1.2 ± 0.3 | 397 ± 16 | 3615 ± 1563 | 4 |
| | | (0.66 ± 0.09) | (0.19 ± 0.11) | (0.20 ± 0.04) | (0.51 ± 0.10) | (0.24 ± 0.08) | (0.23 ± 0.04) | (0.99 ± 0.01) | (0.96 ± 0.02) | |
| | 50 | 31 ± 12 | 3.0 ± 1.6 | 0.12 ± 0.04 | 0.03 ± 0.01 | 0.08 ± 0.03 | 1.0 ± 0.7 | 477 ± 57 | 1013 ± 367 | 4 |
| | | (0.44 ± 0.16) | (0.29 ± 0.18) | (0.28 ± 0.05) | (0.44 ± 0.22) | (0.49 ± 0.25) | (0.06 ± 0.04) | (0.99 ± 0.01) | (0.99 ± 0.01) | |
| Thymol | | | | | | | | | | |
| | 5 | 34 ± 8 | 1.6 ± 1.1 | 0.07 ± 0.06 | 0.02 ± 0.01 | 0.14 ± 0.03 | 1.9 ± 0.7 | 392 ± 200 | 1539 ± 771 | 4 |
| | | (0.58 ± 0.22) | (0.32 ± 0.16) | (0.09 ± 0.03) | (0.70 ± 0.12) | (0.14 ± 0.07) | (0.14 ± 0.07) | (0.99 ± 0.01) | (0.99 ± 0.01) | |
| | 10 | 17 ± 2 | 2.2 ± 0.8 | 0.12 ± 0.07 | 0.03 ± 0.01 | 0.19 ± 0.14 | 0.9 ± 0.3 | 110 ± 80 | 1226 ± 459 | 3 |
| | | (0.27 ± 0.19) | (0.47 ± 0.03) | (0.27 ± 13) | (0.60 ± 0.27) | (0.27 ± 0.14) | (0.15 ± 0.10) | (0.99 ± 0.01) | (0.97 ± 0.02) | |
| | 20 | 34 ± 14 | 0.60 ± 0.40 | 0.05 ± 0.02 | 0.04 ± 0.01 | 0.25 ± 0.11 | 2.1 ± 1.6 | 313 ± 51 | 1761 ± 495 | 5 |
| | | (0.32 ± 0.14) | (0.30 ± 0.16) | (0.43 ± 0.18) | (0.43 ± 0.23) | (0.46 ± 0.07) | (0.08 ± 0.03) | (0.99 ± 0.01) | (0.98 ± 0.01) | |
| | 50 | 45 ± 12 | 1.3 ± 0.7 | 0.06 ± 0.02 | 0.02 ± 0.01 | 0.13 ± 0.06 | 2.2 ± 1.5 | 546 ± 247 | 1215 ± 184 | 3 |
| | | (0.32 ± 0.12) | (0.23 ± 0.09) | (0.44 ± 0.19) | (0.39 ± 0.12) | (0.43 ± 0.06) | (0.13 ± 0.06) | (0.98 ± 0.01) | (0.97 ± 0.01) | |
| | 100 | 39 ± 15 | 1.9 ± 1.5 | 0.11 ± 0.02 | 0.02 ± 0.01 | 0.13 ± 0.03 | 1.9 ± 1.3 | 531 ± 139 | 1581 ± 803 | 6 |
| | | (0.54 ± 0.13) | (0.32 ± 0.13) | (0.14 ± 0.03) | (0.66 ± 0.22) | (0.28 ± 0.17) | (0.08 ± 0.06) | (0.99 ± 0.01) | (0.98 ± 0.01) | |
| Tryptamine | 50 | | | | | | | | | |
| Carvacrol | 10 | | | | | | | | | |
| | | 4.4 ± 1.1[a,b] | 0.07 ± 0.02 | — | 0.03 ± 0.01 | 0.18 ± 0.08 | 1.4 ± 0.9 | 232 ± 151 | 1861 ± 890[c,d] | 6 |
| | | (0.83 ± 0.11) | (0.16 ± 0.11) | — | (0.77 ± 0.17) | (0.18 ± 0.14) | (0.04 ± 0.02) | (0.97 ± 0.01) | (0.96 ± 0.02) | |
| Tryptamine | 50 | | | | | | | | | |
| Thymol | 10 | | | | | | | | | |
| | | 2.7 ± 0.1[a,e] | 0.20 ± 0.16 | — | 0.04 ± 0.01 | 0.31 ± 0.11 | 1.7 ± 0.7 | 120 ± 100 | 560 ± 445[c,f] | 3 |
| | | (0.72 ± 0.04) | (0.28 ± 0.03) | — | (0.79 ± 0.11) | (0.13 ± 0.06) | (0.06 ± 0.05) | (0.96 ± 0.01) | (0.94 ± 0.02) | |

Single-channel currents were recorded at −70 mV in the presence of the ligands at the indicated concentrations. $\tau_{OB}$, $\tau_{OI}$, and $\tau_{OL}$, and $\tau_{CB}$, $\tau_{CI}$, and $\tau_{CL}$ correspond to the mean durations of the brief, intermediate, and long components of open- and closed-time distributions, respectively. Burst duration, cluster duration, and $P_{open}$ were obtained by the K-Means algorithm in QuB after chopping the recording on the base of the corresponding critical time as described in Materials and Methods. $P_{open}$ corresponds to the open probability within a cluster. *n* is the number of recordings for each condition. rel, relative.

[a] $p > 0.05$ with respect to tryptamine.
[b] $p < 0.01$ with respect to carvacrol.
[c] $p < 0.01$ with respect to tryptamine.
[d] $p > 0.05$ with respect to carvacrol.
[e] $p < 0.01$ with respect to thymol.
[f] $p > 0.05$ with respect to thymol. The data correspond to the mean ± SD.

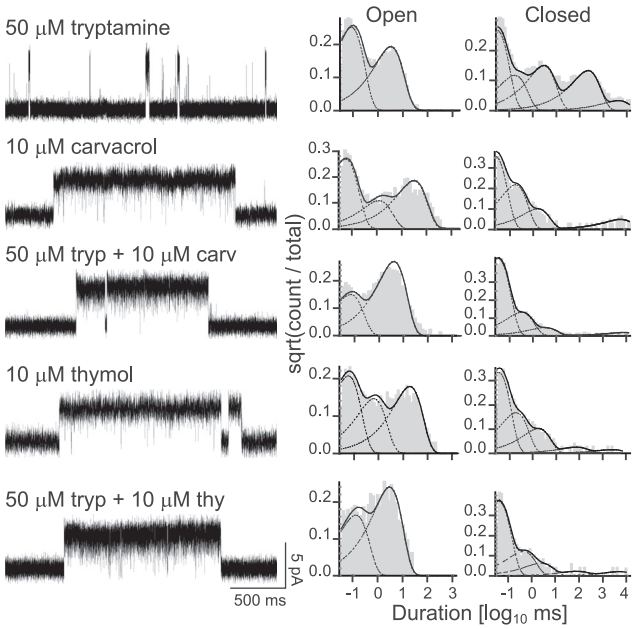


FIGURE 4 Single-channel activity of tryptamine-elicited channels in the presence of carvacrol or thymol. The typical single-channel traces obtained in the cell-attached configuration at −70 mV membrane potential in the presence of tryptamine alone or together with carvacrol or thymol at the indicated concentrations are shown. Typical open- and closed-time histograms are shown. The filter is 9 kHz. Channel openings are shown as upward deflections.

a reduction of the open duration of terpenoid-elicited events.

## Kinetic modeling for activation by orthosteric and allosteric ligands

To generate a kinetic model that describes allosteric activation of the human 5-HT$_3$A receptor, we performed single-channel kinetic analysis. The study was carried out with bursts (for tryptamine) and clusters (for 5-HT and terpenoids) because they provide information of dwell times in open and closed states of a single receptor molecule (see Materials and Methods).

As described above, single-channel activity elicited by 5-HT or allosteric ligands occurred as long-duration clusters composed by bursts separated by interburst/intracluster closings, which correspond to the third component of the closed-time histogram. In contrast, in the presence of tryptamine mainly isolated bursts were detected.

Considering the fact that the single-channel pattern of human 5-HT$_3$A is qualitatively similar to that of the mouse receptor (15), we took advantage of our previous kinetic model generated for the orthosteric activation of the mouse 5-HT$_3$A receptor to describe the human 5-HT$_3$A receptor activation (*scheme 1* in Fig. 5).

Because of the lack of 5-HT concentration dependence of clusters, it was possible to infer that they correspond to activation episodes of receptors that have reached the most favorable occupation state (C), which was previously proposed to be three binding sites (14,15,45). Therefore, scheme 1 is a subset of a complete activation scheme because it does not contain the agonist association and dissociation steps (15). Scheme 1 involves three open states, which were well detected from single-channel recordings, and includes three preopen-closed states ($C_1$, $C_2$, and $C_3$), from which channel opening is allowed. The ability to make the transition to these states (priming) has been associated to the efficacy of the agonists on nicotinic and glycine receptors (19,46).

We first fitted the scheme 1 to clusters obtained from single-channel recordings in the presence of a range of 5-HT concentrations using the MIL algorithm from the QuB Software (see Materials and Methods). Because a reduction in open-time duration was observed with the increase in 5-HT concentration due to open-channel blockade, we connected a block state to the longest-duration open state (B, Fig. 5) and fitted the scheme to a set of single-channel recordings obtained at different agonist concentrations. Although the model includes four closed states, only three intracluster closings were distinguished from the closed-time histograms probably because of the overlap of their durations. Also, we have previously shown for the mouse 5-HT$_3$A receptor that four closed states were required to adequately describe the combined single-channel and macroscopic data (15). The theoretical curves, resulting from fitting the kinetic scheme to the global data set by the maximal likelihood method, well described the experimental open-time and closed-time histograms (Fig. 5 *C*). The estimated rates and constants, shown in Table 2, indicated that: 1) the closed state C (in *scheme 1*) can be associated to dwell times in closed states between bursts and within clusters (Table 2; (15)), 2) the opening rate from the three-primed receptor is the fastest ($\beta_3$, Table 2), and 3) the gating equilibrium constant increases with priming ($\theta_3 > \theta_2 > \theta_1$) (Table 2).

Scheme 1 could not describe tryptamine activation because only two open states were detected, and activation occurred as isolated bursts. Because the interburst/intracluster closings (C in *scheme 1*) were associated to the first priming step, we used a subset version of scheme 1 lacking this transition (*scheme 2* in Fig. 5 *B*) and containing only two open states. The scheme also considered that the longest-duration open state is the most likely to be blocked by the agonist, similar to that observed for 5-HT. This scheme well described the experimental open and closed-duration histograms (Fig. 5 *D*). In line with our previous observations for the mouse 5-HT$_3$A receptor (15), the main difference of tryptamine activation respect to 5-HT activation was the lack of information about the first priming step. This difference may arise from the fact that the longer closings corresponding to this state

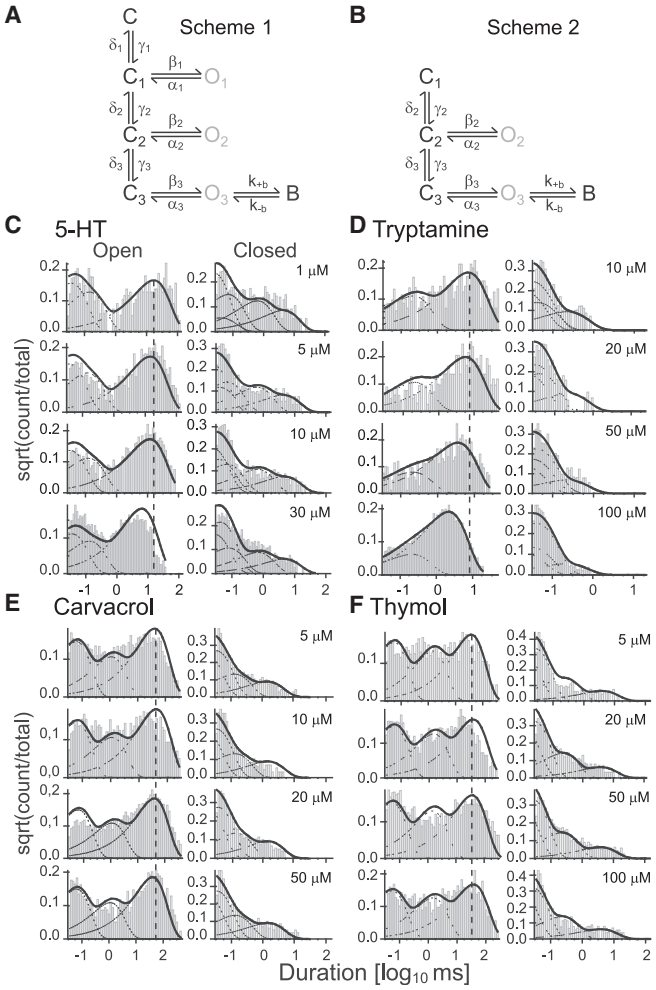


FIGURE 5 Kinetic analysis for 5-$HT_3A_{HC}$ receptor activated by the different agonists. Schemes used for kinetic analysis of clusters (*scheme 1*, *A*) or bursts (*scheme 2*, *B*). Kinetic analysis was restricted to clusters for 5-HT (*C*), carvacrol (*E*), or thymol (*F*), or to bursts for tryptamine (*D*). Scheme 1 shows an interburst/intracluster closed state (state C), three preopen closed states ($C_1$, $C_2$ and $C_3$), three open states ($O_1$, $O_2$ and $O_3$) and a blocked state B. Scheme 2 is a subset of scheme 1 restricted to bursts. The experimental open- and closed-duration histograms from selected clusters or bursts at different agonist concentrations are shown with the theoretical curves superimposed (resulting from fitting the corresponding scheme to the data).

(C in *scheme 1*, Fig. 5 *A*) cannot be distinguished from our single-channel recordings because they overlap with closed times corresponding to independent activation episodes. The results also showed slightly reduced stability of the longest-duration open state compared to 5-HT ($\alpha_3$, Table 2). Thus, reduced priming and, to a lesser extent, decreased open stability explains the weak agonist activity of tryptamine.

We finally determined the kinetics of 5-$HT_3A_{HC}$ channels activated by the allosteric agonists. Because the activation profile was very similar to that of 5-HT, we used scheme 1 to perform kinetic analysis, but we did not include the blockade because this was not evidenced at the range of concentrations used (Fig. S2; Table 1). For allosteric activation, scheme 1 well described the experimental open and closed-time histograms for both compounds (Fig. 5, *E* and *F*). The kinetic analysis revealed similar priming equilibrium constants ($P$) and increased gating equilibrium constants ($\theta_1$, $\theta_2$, and $\theta_3$) with respect to 5-HT activation (Table 2), indicating higher efficacy.

Thus, the kinetic analysis suggests that the mechanism of activation by both orthosteric and allosteric binding sites requires preopen-closed states from which the receptor can open. Compared to 5-HT activation, the main difference is the slightly greater gating equilibrium constant ($\theta$) for both allosteric agonists and reduced priming for tryptamine, which is in line with our previous report (15). Among ligands, the analysis revealed that 1) the equilibrium constants for the second and third priming transitions were similar among the different agonists ($P_2$ and $P_3$ in Table 2), 2) the gating equilibrium constant increased with priming for all ligands ($\theta_3 > \theta_2 > \theta_1$), and 3) the gating equilibrium constant for the most stable open state ($\theta_3$) is slightly different for the different agonists (tryptamine $<$ 5-HT $<$ carv $\approx$ thy).

## DISCUSSION

We here defined the mechanistic bases underlying differences between orthosteric and allosteric activation and potentiation in the least explored Cys-loop receptor, the human 5-$HT_3A$ receptor.

The fact that Cys-loop receptors are important drug targets for a great number of disorders has prompted attention to deciphering the mechanisms of drug modulation. Pharmacological modulation can be achieved through both orthosteric and allosteric sites, resulting in a great spectrum of chemical structures, sites, and mechanisms. Several ago-PAMs of Cys-loop receptors are established therapeutic drugs, such as the anesthetic pentobarbital acting at GABA receptors (47), and the anthelmintic ivermectin acting at the invertebrate glutamate-activated chloride channels (48). The discovery of allosteric ligands of 5-$HT_3A$ receptors for clinical applications has lagged behind compared to that of other Cys-loop receptors. However, compounds acting as negative allosteric modulators have been proposed as drugs or lead structures for reducing chemotherapy-induced nausea and vomiting (26,49). Also, compounds acting as allosteric agonists have been shown to induce antinociception (50). Thus, our study provides novel, to our knowledge, useful information to advance in this relatively unexplored area.

Electrophysiological and structural studies have provided information regarding mechanisms of activation through orthosteric sites, identified structures, and proposed pathways involved (36,45,51,52). However, mechanisms of

**TABLE 2 Kinetic Parameters of Allosteric and Orthosteric 5-HT$_3$A$_{HC}$ Activation**

| | | 5-HT | Tryptamine | Carvacrol | Thymol |
|---|---|---|---|---|---|
| $\gamma_1$ | [$s^{-1}$] | 352 ± 17 | — | 1120 ± 45 | 343 ± 20 |
| $\delta_1$ | [$s^{-1}$] | 419 ± 35 | — | 2362 ± 159 | 759 ± 63 |
| $\gamma_2$ | [$s^{-1}$] | 920 ± 45 | 6035 ± 262 | 2092 ± 96 | 1708 ± 73 |
| $\delta_2$ | [$s^{-1}$] | 5430 ± 304 | 6484 ± 519 | 5160 ± 255 | 4565 ± 222 |
| $\gamma_3$ | [$s^{-1}$] | 4230 ± 300 | 10,100 ± 639 | 15,700 ± 786 | 13,800 ± 655 |
| $\delta_3$ | [$s^{-1}$] | 6244 ± 245 | 6161 ± 533 | 11,000 ± 794 | 13,900 ± 1,260 |
| $\beta_1$ | [$s^{-1}$] | 1601 ± 83 | — | 7126 ± 321 | 5191 ± 215 |
| $\alpha_1$ | [$s^{-1}$] | 30,000 ± 1056 | — | 21,100 ± 650 | 23,300 ± 969 |
| $\beta_2$ | [$s^{-1}$] | 8070 ± 340 | 28,300 ± 2490 | 17,300 ± 760 | 28,700 ± 1292 |
| $\alpha_2$ | [$s^{-1}$] | 9291 ± 341 | 9541 ± 741 | 1416 ± 86 | 1397 ± 96 |
| $\beta_3$ | [$s^{-1}$] | 38,400 ± 1080 | 45,100 ± 1887 | 53,800 ± 2260 | 71,100 ± 4280 |
| $\alpha_3$ | [$s^{-1}$] | 165 ± 5 | 379 ± 21 | 99 ± 4 | 145 ± 11 |
| $P_1$ | | 0.84 ± 0.08 | — | 0.47 ± 0.04 | 0.45 ± 0.05 |
| $P_2$ | | 0.17 ± 0.01 | 0.93 ± 0.08 | 0.41 ± 0.03 | 0.37 ± 0.02 |
| $P_3$ | | 0.68 ± 0.05 | 1.6 ± 0.2 | 1.4 ± 0.1 | 1.0 ± 0.1 |
| $\theta_1$ | | 0.05 ± 0.01 | — | 0.34 ± 0.02 | 0.22 ± 0.01 |
| $\theta_2$ | | 0.87 ± 0.05 | 2.9 ± 0.4 | 12 ± 1 | 21 ± 2 |
| $\theta_3$ | | 233 ± 10 | 119 ± 8 | 543 ± 32 | 490 ± 47 |
| $k_{+B}$ | [$M^{-1}$ $s^{-1}$] × $10^6$ | 6.8 ± 0.3 | 8.2 ± 0.2 | — | — |
| $k_{-B}$ | [$s^{-1}$] | 27,800 ± 1078 | 26,900 ± 438 | — | — |

Rates are expressed in $s^{-1}$. Kinetics parameters were obtained from clusters using scheme 1 (5-HT, carvacrol, and thymol) or from bursts using scheme 2 (tryptamine). The rates are expressed as mean ± SE for three different patches for each condition. The equilibrium constants are $P$ ($\gamma/\delta$) for priming and $\theta$ ($\beta/\alpha$) for gating.

allosteric activation remain less understood and have not been addressed at all in 5-HT$_3$ receptors.

For 5-HT$_3$A, activation at the single-channel level can only be studied using the high-conductance, triple-mutant receptor because its low-channel amplitude does not allow detection of opening events from cell-attached patches. We here showed that the macroscopic activation properties of the human high-conductance receptor are similar to those of the wild-type receptor. Moreover, single-channel studies of the chimeric receptor containing $\alpha$7 sequence in the extracellular domain and 5-HT$_3$A in the transmembrane domain ($\alpha$7-5HT$_3$A) (53), and the $\alpha$7 nicotinic receptor (54) have demonstrated that the mutations of the three residues change conductance but do not affect single-channel kinetics of the receptors. Thus, our high-conductance form of the human 5-HT$_3$A receptor is a valid model for defining kinetics.

The single-channel activity of the high-conductance form of the human 5-HT$_3$A receptor has not been described before. We found that channel amplitude is similar to that of the high-conductance mouse 5-HT$_3$A receptor and its single-channel activation pattern also maintains the main features of that of the mouse receptor: long clusters, high $P_{open}$ within clusters and no agonist concentration dependence (14). A main feature of 5-HT$_3$A receptor activation is that the increase in 5-HT concentration from 1 to 10 $\mu$M increases the macroscopic response from ~25 to ~85%, whereas it does not affect the single-channel pattern, which, in turn, shows the same clusters of ~300 ms and $P_{open}$ of ~0.9 at the 10-fold concentration range. These findings indicate that clusters do not include agonist association and dissociation steps. Thus, the observed agonist concentration dependence of the macroscopic responses may be due to the increase in the frequency of individual clusters with agonist concentration. A similar behavior has been reported for other Cys-loop receptors (55–57).

We found that the same model proposed for the mouse 5-HT$_3$A (15) well described the experimental data of the human type receptor elicited by the full agonist 5-HT and the partial agonist tryptamine as well as for allosteric ligands.

As we used clusters to define kinetics, our model does not include binding steps. This model includes preactivated states (primed states); the ability to make the transition to these states (priming) has been associated to the efficacy of other Cys-loop receptors (18,19). Interestingly, a preactive state was suggested by cryo-electron microscopy of the full length 5-HT$_3$A (35).

The kinetic analysis for 5-HT activation revealed similar priming equilibrium constants between mouse and human receptors ($P_1$, $P_2$, and $P_3$ were ~0.5, ~0.6, and ~0.5 for mouse, and 0.8, 0.2, and 0.7 for human) (Table 2; (15)). However, with respect to the mouse receptor, the human receptor showed smaller gating equilibrium constants, which were about one order of magnitude lower ($\theta_1$, $\theta_2$, and $\theta_3$ were ~0.05, ~0.9, and ~230 for human, and ~0.2, ~3, and ~1800 for mouse, respectively) (Table 2; (15)).

As allosteric agonists, we used terpenoids that are monocyclic phenolic compounds present in essential oils from aromatic plants widely used in traditional medicine (58). At the molecular level, they exert multiple effects throughout the Cys-loop receptor family in both vertebrates and invertebrates, including activation, potentiation, and inhibition (59,60). In 5-HT$_3$A receptors, terpenoids have been shown to act as either ago-PAMs or allosteric inhibitors. In

particular, by macroscopic current recordings it was shown that carvacrol and thymol act as partial agonists and potentiators of 5-$HT_3$A receptors (31). Docking and functional studies have proposed that the binding site of thymol is located in an intersubunit cavity in the transmembrane region (31).

Our results confirmed that carvacrol and thymol macroscopically behave as agonists with lower efficacy than 5-HT because currents show submaximal amplitudes and significantly slower rising phases. However, macroscopic current recordings for ligand-gated ion channels cannot separate binding from gating steps and do not consider other mechanisms, such as open-channel block, that can result in reduced maximal responses (61). In contrast, at the microscopic level, we found that terpenoids activate 5-$HT_3$A receptors even more efficaciously than 5-HT, which is evidenced by similar equilibrium constants for priming ($P_1$, $P_2$, and $P_3$) and higher for gating ($\theta_1$, $\theta_2$, and $\theta_3$). Also, single-channel kinetic analysis revealed that activation can be described by a similar mechanism as that of orthosteric activation. Moreover, the kinetic scheme is different to that in the presence of tryptamine, which is a genuine partial agonist, for which it was not possible to estimate the value of $P_1$ and $\theta_1$. Thus, this study enhances the importance of single-channel kinetic studies for understanding drug action on ligand-gated ion channels.

We analyzed possible explanations for the apparent discrepancy of terpenoid activity between the macroscopic level (submaximal and slower responses) and the single-channel level (long-duration and high-$P_{open}$ clusters). It is known that open-channel blockade elicited by the agonist at high concentrations may reduce the maximal macroscopic responses (61). This mechanism has explained the low efficacy of 2-methyl-5-hydroxytryptamine for mouse 5-$HT_3$A receptors (15). However, we did not detect a clear reduction in open duration, cluster duration, and $P_{open}$ within clusters at high carvacrol or thymol concentrations, indicating no channel blockade and, therefore, we can discard blockade as mediating submaximal macroscopic responses.

Also, the formation of primed, intermediate states from which channel opening rapidly occurs was similar for 5-HT and terpenoids, but was different for the orthosteric partial agonist, tryptamine. Thus, slow priming can explain the reduced efficacy observed at the macroscopic level for tryptamine but not for terpenoids (15,18,19).

The possibility of describing the activation by allosteric agonists by the same mechanism as that for orthosteric agonists led us to inquire if allosteric ligands also elicit structural changes at the binding site. Structural and computational studies in Cys-loop receptors suggested that the C-loop, which is one of the three loops that form the principal face of the binding site, adopts an opened-up, uncapped conformation in the absence of agonist and it closes to cap the agonist, an event associated with priming and channel opening. Orthosteric partial agonists produce incomplete closure in line with their reduced priming (19,56,62–67). There is no experimental information regarding closing of the C-loop by allosteric agonists. However, computational studies using a homology model of the $\alpha$7 nicotinic receptor showed that an allosteric agonist affected the conformational freedom of C-loop and produced channel activation by a cross-talk between the allosteric and the orthosteric sites (68). Moreover, a study using a Gaussian method model in 23 proteins demonstrated that the motions of allosteric sites are highly correlated with the motions of orthosteric sites (69). Thus, it may be possible that despite binding to the transmembrane site, terpenoids allosterically induce the closing of the C-loop located at the extracellular domain.

Another possible explanation for the discrepancy between macroscopic and microscopic observations is the accessibility of terpenoids to the allosteric binding sites through the membrane, which probably leads to the slow-rising phase of macroscopic currents, as determined for the allosteric activation by ivermectin of glutamate-activated chloride channels (70). Experimental and computational studies have shown that thymol and carvacrol incorporate into the lipid membrane in a saturable manner and that thymol in water solution tends to self-aggregate when the concentration increases over a critical value (31,71–74). In addition, the number of allosteric sites required for activation may differ from that of orthosteric sites, as previously determined for allosteric agonists of GABA receptors (75). Thus, maximal saturation of the allosteric sites may not occur under the conditions used for whole-cell recordings, but it may occur during the longer, steady-state, single-channel current measurements.

Overall, our findings showed the first single-channel characterization of the activation of the human 5-$HT_3$A receptor by allosteric ligands, which are of increasing interest as research and therapeutic tools for all the Cys-loop receptor family.

## SUPPORTING MATERIAL

Supporting Material can be found online at https://doi.org/10.1016/j.bpj.2020.08.029.

## AUTHOR CONTRIBUTIONS

J.C. and C.B. designed the work. C.F., N.R.A., A.M.D., and J.C. performed experiments. C.F., N.R.A., A.M.D., J.C., and C.B. analyzed data. J.C. and C.B. wrote the article.

## ACKNOWLEDGMENTS

This work was supported by grants from the National Research Council of Argentina, Universidad Nacional del Sur, and Agencia Nacional de Promoción Científica y Tecnológica from Argentina to C.B. and J.C.

## REFERENCES


1. Kelley, S. P., J. I. Dunlop, …, J. A. Peters. 2003. A cytoplasmic region determines single-channel conductance in 5-HT$_3$ receptors. *Nature.* 424:321–324.
2. Corradi, J., and C. Bouzat. 2016. Understanding the bases of function and modulation of α7 nicotinic receptors: implications for drug discovery. *Mol. Pharmacol.* 90:288–299.
3. Pandhare, A., E. Pirayesh, …, M. Jansen. 2019. Triple arginines as molecular determinants for pentameric assembly of the intracellular domain of 5-HT $_{3A}$ receptors. *J. Gen. Physiol.* 151:1135–1145.
4. Juza, R., P. Vlcek, …, J. Korabecny. 2020. Recent advances with 5-HT $_3$ modulators for neuropsychiatric and gastrointestinal disorders. *Med. Res. Rev.* 40:1593–1678.
5. Niesler, B., J. Walstab, …, M. Brüss. 2007. Characterization of the novel human serotonin receptor subunits 5-HT3C,5-HT3D, and 5-HT3E. *Mol. Pharmacol.* 72:8–17.
6. Niesler, B. 2011. 5-HT($_3$) receptors: potential of individual isoforms for personalised therapy. *Curr. Opin. Pharmacol.* 11:81–86.
7. Price, K. L., Y. Hirayama, and S. C. R. Lummis. 2017. Subtle differences among 5-HT $_3$ AC, 5-HT $_3$ AD, and 5-HT $_3$ AE receptors are revealed by partial agonists. *ACS Chem. Neurosci.* 8:1085–1091.
8. Maricq, A. V., A. S. Peterson, …, D. Julius. 1991. Primary structure and functional expression of the 5HT$_3$ receptor, a serotonin-gated ion channel. *Science.* 254:432–437.
9. Hope, A. G., J. A. Peters, …, T. P. Blackburn. 1996. Characterization of a human 5-hydroxytryptamine3 receptor type A (h5-HT$_3$R-AS) subunit stably expressed in HEK 293 cells. *Br. J. Pharmacol.* 118:1237–1245.
10. Davies, P. A., M. Pistis, …, E. F. Kirkness. 1999. The 5-HT3B subunit is a major determinant of serotonin-receptor function. *Nature.* 397:359–363.
11. Brady, C. A., I. M. Stanford, …, N. M. Barnes. 2001. Pharmacological comparison of human homomeric 5-HT$_{3A}$ receptors versus heteromeric 5-HT$_{3A/3B}$ receptors. *Neuropharmacology.* 41:282–284.
12. Corradi, J., A. J. Thompson, …, S. C. R. Lummis. 2015. 5-HT$_3$ receptor brain-type B-subunits are differentially expressed in heterologous systems. *ACS Chem. Neurosci.* 6:1158–1164.
13. Peters, J. A., J. E. Carland, …, J. J. Lambert. 2006. Novel structural determinants of single-channel conductance in nicotinic acetylcholine and 5-hydroxytryptamine type-3 receptors. *Biochem. Soc. Trans.* 34:882–886.
14. Corradi, J., F. Gumilar, and C. Bouzat. 2009. Single-channel kinetic analysis for activation and desensitization of homomeric 5-HT($_3$)A receptors. *Biophys. J.* 97:1335–1345.
15. Corradi, J., and C. Bouzat. 2014. Unraveling mechanisms underlying partial agonism in 5-HT$_3$A receptors. *J. Neurosci.* 34:16865–16876.
16. Corradi, J., N. Andersen, and C. Bouzat. 2011. A novel mechanism of modulation of 5-HT$_3$A receptors by hydrocortisone. *Biophys. J.* 100:42–51.
17. Mott, D. D., K. Erreger, …, S. F. Traynelis. 2001. Open probability of homomeric murine 5-HT$_3$A serotonin receptors depends on subunit occupancy. *J. Physiol.* 535:427–443.
18. Lape, R., D. Colquhoun, and L. G. Sivilotti. 2008. On the nature of partial agonism in the nicotinic receptor superfamily. *Nature.* 454:722–727.
19. Mukhtasimova, N., W. Y. Lee, …, S. M. Sine. 2009. Detection and trapping of intermediate states priming nicotinic receptor channel opening. *Nature.* 459:451–454.
20. Sivilotti, L., and D. Colquhoun. 2016. In praise of single channel kinetics. *J. Gen. Physiol.* 148:79–88.
21. Gilmore, J., S. D'Amato, …, L. Schwartzberg. 2018. Recent advances in antiemetics: new formulations of 5HT $_3$-receptor antagonists. *Cancer Manag. Res.* 10:1827–1857.
22. Walstab, J., G. Rappold, and B. Niesler. 2010. 5-HT($_3$) receptors: role in disease and target of drugs. *Pharmacol. Ther.* 128:146–169.
23. Baptista-Hon, D. T., T. Z. Deeb, …, T. G. Hales. 2012. The 5-HT3B subunit affects high-potency inhibition of 5-HT$_3$ receptors by morphine. *Br. J. Pharmacol.* 165:693–704.
24. Wetzel, C. H., B. Hermann, …, R. Rupprecht. 1998. Functional antagonism of gonadal steroids at the 5-hydroxytryptamine type 3 receptor. *Mol. Endocrinol.* 12:1441–1451.
25. Oz, M. 2006. Receptor-independent effects of endocannabinoids on ion channels. *Curr. Pharm. Des.* 12:227–239.
26. Al Kury, L. T., M. Mahgoub, …, M. Oz. 2018. Natural negative allosteric modulators of 5-HT$_3$ receptors. *Molecules.* 23:3186.
27. Jarvis, G. E., R. Barbosa, and A. J. Thompson. 2016. Noncompetitive inhibition of 5-HT$_3$ receptors by citral, linalool, and eucalyptol revealed by nonlinear mixed-effects modeling. *J. Pharmacol. Exp. Ther.* 356:549–562.
28. Lovinger, D. M., and Q. Zhou. 1998. Alcohol effects on the 5-HT$_3$ ligand-gated ion channel. *Toxicol. Lett.* 100–101:239–246.
29. van Hooft, J. A., E. van der Haar, and H. P. Vijverberg. 1997. Allosteric potentiation of the 5-HT$_3$ receptor-mediated ion current in N1E-115 neuroblastoma cells by 5-hydroxyindole and analogues. *Neuropharmacology.* 36:649–653.
30. Newman, A. S., N. Batis, …, N. M. Barnes. 2013. 5-Chloroindole: a potent allosteric modulator of the 5-HT$_3$ receptor. *Br. J. Pharmacol.* 169:1228–1238.
31. Lansdell, S. J., C. Sathyaprakash, …, N. S. Millar. 2015. Activation of human 5-hydroxytryptamine type 3 receptors via an allosteric transmembrane site. *Mol. Pharmacol.* 87:87–95.
32. Ziemba, P. M., B. S. P. Schreiner, …, G. Gisselmann. 2015. Activation and modulation of recombinantly expressed serotonin receptor type 3A by terpenes and pungent substances. *Biochem. Biophys. Res. Commun.* 467:1090–1096.
33. Ashoor, A., J. C. Nordman, …, M. Oz. 2013. Menthol inhibits 5-HT$_3$ receptor-mediated currents. *J. Pharmacol. Exp. Ther.* 347:398–409.
34. Chatzidaki, A., and N. S. Millar. 2015. Allosteric modulation of nicotinic acetylcholine receptors. *Biochem. Pharmacol.* 97:408–417.
35. Polovinkin, L., G. Hassaine, …, H. Nury. 2018. Conformational transitions of the serotonin 5-HT $_3$ receptor. *Nature.* 563:275–279.
36. Gielen, M., and P. J. Corringer. 2018. The dual-gate model for pentameric ligand-gated ion channels activation and desensitization. *J. Physiol.* 596:1873–1902.
37. Hassaine, G., C. Deluz, …, H. Nury. 2014. X-ray structure of the mouse serotonin 5-HT$_3$ receptor. *Nature.* 512:276–281.
38. Bouzat, C., F. Gumilar, …, S. M. Sine. 2004. Coupling of agonist binding to channel gating in an ACh-binding protein linked to an ion channel. *Nature.* 430:896–900.
39. Qin, F., A. Auerbach, and F. Sachs. 1996. Estimating single-channel kinetic parameters from idealized patch-clamp data containing missed events. *Biophys. J.* 70:264–280.
40. Qin, F., A. Auerbach, and F. Sachs. 1997. Maximum likelihood estimation of aggregated Markov processes. *Proc. Biol. Sci.* 264:375–383.
41. Purohit, Y., and C. Grosman. 2006. Estimating binding affinities of the nicotinic receptor for low-efficacy ligands using mixtures of agonists and two-dimensional concentration-response relationships. *J. Gen. Physiol.* 127:719–735.
42. Brett, R. S., J. P. Dilger, …, B. Lancaster. 1986. A method for the rapid exchange of solutions bathing excised membrane patches. *Biophys. J.* 50:987–992.
43. Meiboom, M. F., M. Barann, …, B. W. Urban. 2013. Which agonist properties are important for the activation of 5-HT$_3$A receptors? *Biochim. Biophys. Acta.* 1828:2564–2573.
44. Neher, E., and J. H. Steinbach. 1978. Local anaesthetics transiently block currents through single acetylcholine-receptor channels. *J. Physiol.* 277:153–176.
45. Solt, K., D. Ruesch, …, D. E. Raines. 2007. Differential effects of serotonin and dopamine on human 5-HT$_3$A receptor kinetics: interpretation within an allosteric kinetic model. *J. Neurosci.* 27:13151–13160.

46. Lape, R., A. J. R. Plested, …, L. G. Sivilotti. 2012. The α1K276E startle disease mutation reveals multiple intermediate states in the gating of glycine receptors. *J. Neurosci.* 32:1336–1352.

47. Muroi, Y., C. M. Theusch, …, M. B. Jackson. 2009. Distinct structural changes in the $GABA_A$ receptor elicited by pentobarbital and GABA. *Biophys. J.* 96:499–509.

48. Lynagh, T., and J. W. Lynch. 2012. Ivermectin binding sites in human and invertebrate Cys-loop receptors. *Trends Pharmacol. Sci.* 33:432–441.

49. Pertz, H. H., J. Lehmann, …, S. Elz. 2011. Effects of ginger constituents on the gastrointestinal tract: role of cholinergic M3 and serotonergic $5\text{-}HT_3$ and $5\text{-}HT_4$ receptors. *Planta Med.* 77:973–978.

50. Ferreira Junior, W. A., A. J. Zaharenko, …, Y. Cury. 2017. Peripheral $5\text{-}HT_3$ receptors are involved in the antinociceptive effect of bunodosine 391. *Toxins (Basel).* 10:12.

51. Sauguet, L., A. Shahsavar, …, M. Delarue. 2014. Crystal structures of a pentameric ligand-gated ion channel provide a mechanism for activation. *Proc. Natl. Acad. Sci. USA.* 111:966–971.

52. Bouzat, C., and S. M. Sine. 2018. Nicotinic acetylcholine receptors at the single-channel level. *Br. J. Pharmacol.* 175:1789–1804.

53. Rayes, D., M. J. De Rosa, …, C. Bouzat. 2009. Number and locations of agonist binding sites required to activate homomeric Cys-loop receptors. *J. Neurosci.* 29:6022–6032.

54. Andersen, N., J. Corradi, …, C. Bouzat. 2013. Stoichiometry for activation of neuronal α7 nicotinic receptors. *Proc. Natl. Acad. Sci. USA.* 110:20819–20824.

55. Rayes, D., G. Spitzmaul, …, C. Bouzat. 2005. Single-channel kinetic analysis of chimeric alpha7-5HT3A receptors. *Mol. Pharmacol.* 68:1475–1483.

56. Bouzat, C., M. Bartos, …, S. M. Sine. 2008. The interface between extracellular and transmembrane domains of homomeric Cys-loop receptors governs open-channel lifetime and rate of desensitization. *J. Neurosci.* 28:7808–7819.

57. Krashia, P., R. Lape, …, L. G. Sivilotti. 2011. The long activations of α2 glycine channels can be described by a mechanism with reaction intermediates ("flip"). *J. Gen. Physiol.* 137:197–216.

58. Tsuchiya, H. 2017. Anesthetic agents of plant origin: a review of phytochemicals with anesthetic activity. *Molecules.* 22:1369.

59. Price, K. L., and S. C. R. Lummis. 2014. An atypical residue in the pore of Varroa destructor GABA-activated RDL receptors affects picrotoxin block and thymol modulation. *Insect Biochem. Mol. Biol.* 55:19–25.

60. Hernando, G., O. Turani, and C. Bouzat. 2019. *Caenorhabditis elegans* muscle Cys-loop receptors as novel targets of terpenoids with potential anthelmintic activity. *PLoS Negl. Trop. Dis.* 13:e0007895.

61. Colquhoun, D. 1998. Binding, gating, affinity and efficacy: the interpretation of structure-activity relationships for agonists and of the effects of mutating receptors. *Br. J. Pharmacol.* 125:924–947.

62. Gao, F., N. Bren, …, S. M. Sine. 2005. Agonist-mediated conformational changes in acetylcholine-binding protein revealed by simulation and intrinsic tryptophan fluorescence. *J. Biol. Chem.* 280:8443–8451.

63. Unwin, N., and Y. Fujiyoshi. 2012. Gating movement of acetylcholine receptor caught by plunge-freezing. *J. Mol. Biol.* 422:617–634.

64. Lasala, M., J. Corradi, …, C. Bouzat. 2018. A human-specific, truncated α7 nicotinic receptor subunit assembles with full-length α7 and forms functional receptors with different stoichiometries. *J. Biol. Chem.* 293:10707–10717.

65. Miller, P. S., and T. G. Smart. 2010. Binding, activation and modulation of Cys-loop receptors. *Trends Pharmacol. Sci.* 31:161–174.

66. Billen, B., R. Spurny, …, C. Ulens. 2012. Molecular actions of smoking cessation drugs at α4β2 nicotinic receptors defined in crystal structures of a homologous binding protein. *Proc. Natl. Acad. Sci. USA.* 109:9173–9178.

67. Hibbs, R. E., G. Sulzenbacher, …, Y. Bourne. 2009. Structural determinants for interaction of partial agonists with acetylcholine binding protein and neuronal α7 nicotinic acetylcholine receptor. *EMBO J.* 28:3040–3051.

68. Grazioso, G., J. Sgrignani, …, A. Cavalli. 2015. Allosteric modulation of alpha7 nicotinic receptors: mechanistic insight through metadynamics and essential dynamics. *J. Chem. Inf. Model.* 55:2528–2539.

69. Ma, X., H. Meng, and L. Lai. 2016. Motions of allosteric and orthosteric ligand-binding sites in proteins are highly correlated. *J. Chem. Inf. Model.* 56:1725–1733.

70. Atif, M., J. J. Smith, …, A. Keramidas. 2019. GluClR-mediated inhibitory postsynaptic currents reveal targets for ivermectin and potential mechanisms of ivermectin resistance. *PLoS Pathog.* 15:e1007570.

71. Turina, A. V., M. V. Nolan, …, M. A. Perillo. 2006. Natural terpenes: self-assembly and membrane partitioning. *Biophys. Chem.* 122:101–113.

72. Ferreira, J. V. N., T. M. Capello, …, L. Caseli. 2016. Mechanism of action of thymol on cell membranes investigated through lipid Langmuir monolayers at the air-water interface and molecular simulation. *Langmuir.* 32:3234–3241.

73. Ultee, A., E. P. Kets, and E. J. Smid. 1999. Mechanisms of action of carvacrol on the food-borne pathogen Bacillus cereus. *Appl. Environ. Microbiol.* 65:4606–4610.

74. Shapiro, S., and B. Guggenheim. 1995. The action of thymol on oral bacteria. *Oral Microbiol. Immunol.* 10:241–246.

75. Amin, J., and M. S. Subbarayan. 2017. Orthosteric- versus allosteric-dependent activation of the $GABA_A$ receptor requires numerically distinct subunit level rearrangements. *Sci. Rep.* 7:7770.